Neural Comput & Applic (2019) 31:327–336
DOI 10.1007/s00521-017-2990-z

ORIGINAL ARTICLE

An artificial neural network approach for under-reamed piles subjected to uplift forces in dry sand

Hossein Moayedi[1] · **Abbas Rezaei**[2]

Received: 7 December 2016 / Accepted: 28 March 2017 / Published online: 4 April 2017

Abstract The present study is about under-reamed pile subjected to uplift forces. They are known to be very effective especially against uplift forces. The objective is to develop a simple design formula based on an optimized artificial neural network (ANN) predictive approach model. This formula can calculate the ultimate uplift capacity of under-reamed piles (P_{ul}) embedded in dry cohesionless soil with excellent accuracy. The new generated ANN model was developed by taking into account the key factors such as under-reamed base diameter, angle of enlarged base to the vertical axis, shaft diameter, and embedment ratio. The proposed approach shows excellent agreement with a mean absolute error (MAE) less than 0.262, which is better than previous theories.

Keywords Artificial neural network · Under-reamed pile · Uplift force · Dry sand

1 Introduction

Generally, high rise structures like mooring systems for surface, transmission towers, or even high rise/tall buildings are subjected to large lateral loads, huge overturning moments due to waves, wind, or even both, in addition to vertical compressive load. Therefore, the usual bored piles (normally constructed from reinforced concrete) supporting these structures have to struggle with large uplift and lateral moments and loads. In most cases, these moments and loads (lateral, compressive, and uplift) act on the single piles simultaneously [1–3]. There are many theoretical methods available to assess pile behavior under different independent, lateral, vertical uplift, and vertical compressive loadings [4–6]. Under-reamed and/or enlarged base piles are normally constructed from concrete, with a mechanically formed under-reamed (also called belled pile) designed to increase bearing capacity of the pile. Typically, pile base geometry is in the form of an inverted cone. It can be used to provide uplift capacity by forcing a passive failure wedge of soil (normally because of weight of the soil placed above under-reamed pile) to mobilize for failure to occur and increase the compressive base capacity (end bearing capacity) [7].

Numerous field and laboratory works were performed to study the behavior of uplift loaded base pier. However, there are relatively few papers in the technical literature which deal with an under-reamed pier or belled pier resisting uplift load in sand [8–11]. For analyzing purposes, the limiting capacity of under-reamed pier embedded in sand can be carried out based on theoretical and semi empirical work [12, 13]. Full scale tests and laboratory tests on small models were performed in order to obtain appropriate solution [14, 15]. Furthermore, sometimes, a full-scale test was employed to verify the results based on laboratory tests [16]. Sego et al. [9] investigated on end bearing and total capacities of a pile after enlarging base of the pile. The pile was located on ice-rich permafrost. The results clearly proved that total capacity can be substantially improved through the use of belled piles. Honda et al. [17] applied a two-dimensional distinct element (DE) analysis to evaluate the uplift resistance of belled and multi-belled piles embedded in dense sand. As a result and based on the soil movements in DE analysis, a theoretical solution for predicting the uplift resistance of belled and multi-belled piles was generated from an upper bound limit analysis [17]. Chae et al. [18] investigated on

✉ Hossein Moayedi
h.moayedi@kut.ac.ir

[1] Department of Civil Engineering, Kermanshah University of Technology, Kermanshah, Iran

[2] Department of Electrical Engineering, Kermanshah University of Technology, Kermanshah, Iran

the uplift capacity of belled pile in weathered sandstones in a coastal development on the Persian Gulf. They have conducted a series of full-scale pullout load test on belled tension piles in Abu Dhabi, the United Arab Emirates. After comparison of results from field, 3D finite element analysis, and the theoretical methods, it is found that common theoretical methods overestimate ultimate pull out resistance of the belled pile regardless of bell-shape considerations [18]. Yao and Chen [19] established an elastic-plastic analytical solutions for the uplift belled pile. Through the comparison between obtained results from generated solutions and results of theoretical calculation, it was found that elastic-plastic analytical solutions revealed a good approach to the field test results. Lin et al. [20] introduced a new method for estimating the ultimate uplift resistance of under-reamed pile embedded in sandy soil. The differences of new method with conventional methods is that the elastic/plastic behavior of soil around belled pile is being taken into account. Lin et al. [20] performed a series of experimental/field tests to gain development of the failure surface with curved slip-surface. Results illustrated that the starting location of failure surface is developed at a distance away from the pile surface. In several cases, researchers used extra reinforcement materials such as various types of geosynthetics to enhance the rate of uplift bearing capacity [21–23]. For instance, Tafreshi et al. [24] investigated on the enhancement of geocell reinforcement on uplift resistance of belled piles and also in the performance improvement of the uplift bearing capacity of belled pile under repeated tensile and compressive loads. It is observed that the geocell material allowed higher tensile loads or increased cycling. In addition, Tafreshi et al. [24] noted that required length of pile shaft can be reduced using the geocell reinforcement causes to reduce required pile's material, backfill, and excavation.

There are also many studies on using artificial neural network (ANN) in order to predict bearing capacity of pile foundation [25–30], pile dynamic capacity [31, 32], pile setup [33, 34], and pile settlements [35, 36]. For example, Suman et al. [25] used artificial intelligence techniques to predict friction resistance of driven piles in clay using. The prediction models were presented using two recently developed artificial intelligence techniques, functional networks (FN) and multivariate adaptive regression splines (MARS). The models predict friction resistance of piles in clay soils based on experimental test results. Based on statistical performances, MARS and FN models are found to have a better predictive resistance than existing models. Rahman et al. [37] developed an ANN model to predict the uplift capacity of suction foundations using a database containing the results from a number of model and centrifuge tests. Ardalan et al. [38] optimized a group of data handling (GMDH) type neural networks using genetic algorithms (Gas). The model have been used to explore effects of effective cone point resistance and cone sleeve friction as input parameters on pile unit shaft resistance. Alavi et al. [39] utilized a classical tree-based genetic programming (TGP), linear genetic programming (LGP), and gene expression programming (GEP) to develop and formulate new prediction equations for the uplift capacity of suction caissons using an experimental database obtained from published literature. Cheng et al. [40] developed an intelligent fuzzy radial basis function (RBF) neural network inference model (IFRIM), which is a hybrid of RBF neural network, fuzzy logic (FL), and artificial bee colony (ABC) algorithm and has been used to predict the uplift capacity of suction caissons.

To ensure serviceability and stability of the structures, bearing capacities against uplift and horizontal forces are taking into account in the design process of foundations. Unlike the lateral and compression resistance, the uplift capacities of piles with under-reamed has not yet been fully investigated; also, such piles are known to be very effective against uplift force, but research on their uplift behavior has been limited. In the present study, an attempt has been made to develop an optimized ANN-based predictive approach model to calculate the ultimate uplift capacity of under-reamed piles embedded in dry cohesionless soil. In order to develop the new design model, dataset consist of an extensive number of small scale laboratory tests on uplift capacity of under-reamed pile published literature which have been used. We have proposed a novel ANN model to model and predict ultimate uplift capacity of the under-reamed piles embedded in dry cohesionless soil. This model is introduced by us for the first time. This model is an accurate and very fast tool in comparison with the experimental or numerical methods. Also, using the proposed ANN model, an equation is proposed for the first time to relate inputs including base diameter, angle of enlarged base, shaft diameter and embedment ratio, and the output ultimate uplift resistance.

2 Data collection and methodology

Used data to make the ANN model in this study was obtained from the small scale laboratory work conducted in a geotechnical laboratory, performed by Nazir et al. [13]. The purpose of research carried out by Nazir et al. [12] was to determine the bearing capability of an enlarged base pier against uplift forces. Experiments were performed in a large plexiglass box. A total number of 432 laboratory experiments were undertaken in both dense and loose sand condition. Enlarged base piers with base angles of $\alpha = 30°$, $\alpha = 45°$, and $\alpha = 60°$; base diameters between 75 and 150 mm; and pile diameter ranging from 30 to 50 mm were tested. An example of under-reamed base pile and key parameters considered for ANN model is depicted in Fig. 1 while Table 1 illustrated similar design parameters used in the small scale experimental plan as well as proposed ANN approach.

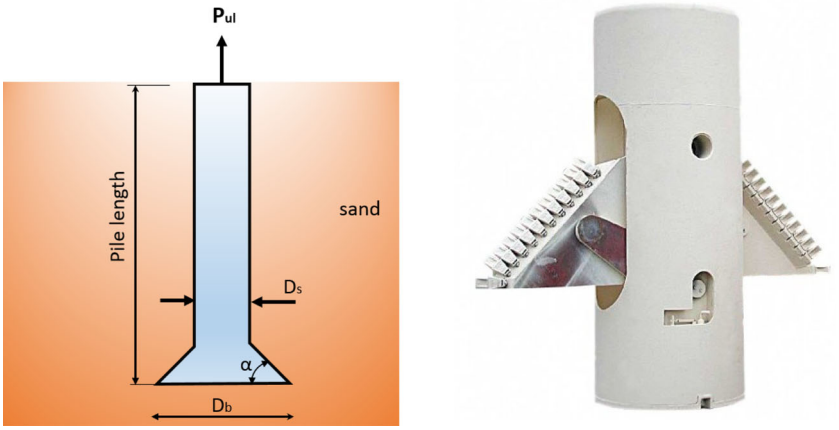

(a) under reamed pile (b) belling bucket

Fig. 1 An example of under-reamed pile. **a** Key parameters. **b** Belling bucket

3 Artificial neural network (ANN)

In the current paper, we optimized an ANN method to model and predict the ultimate uplift capacity of the under-reamed piles embedded in dense and loose dry sand. The new generated ANN model was developed by taking into account the key factors such as base diameter D_b, angle of enlarged base (α), shaft diameter (D_s), and embedment ratio (L/D_b) as the inputs and ultimate uplift resistance (P_{ul}) as the output. For this means, a special type of feed forward network called the multi-layer perceptron (MLP) neural network is used, which is the most widely used ANN. Figure 2a shows the proposed MLP network used in this study. This structure consists of three layers as the input layer, the hidden layer, and the output layer. Each layer basically consists of interconnected neurons (basic processing elements of ANN), in which the synapses of biological neurons are modeled as the weights. The mathematic model of a neuron is shown in Fig. 2b, where $U_1, U_2, \ldots, U_t$ are inputs, b is the bias term, f is the transfer function, and $W_{1,1}$, $W_{1,2}, \ldots, W_{1,t}$ are the connection weights. The output of this neuron is also given by the following equation [41, 42]:

$$O = f\left(\sum_{i=1}^{t}\left(U_i W_{1,i}\right) + b\right) \quad (1)$$

The neurons in input layer transfer inputs to the next layer without any changes. Also, in output layer, the transfer function f is equal to 1. For the hidden layers, the transfer function f is usually tansig function, which is given by the following equation for variable x:

$$\text{Tansig}(x) = \frac{2}{1+e^{-2x}} - 1 \quad (2)$$

The connection weights and bias can be adjusted during the training process using back-propagation training algorithm, which is an error-minimization technique.

In order to find the optimized ANN model, many ANN structures (i.e., using MLP) were tested using 1, 2, and 3 hidden layers. Different number of neurons were considered in each hidden layer. This process continued to obtain an accurate ANN model with the minimum error in both training and testing data set. Besides, the optimized ANN model should have a simple and less complicated structure. After testing large number of ANN structures, the best ANN model structure is found with one hidden layer and 10 neurons in its hidden layer. Noteworthy, developed model possesses 5 neurons in input layer, while 10 neurons in hidden layer, and 1 neurons in output layer. To train and test the proposed ANN model, required data set was obtained from the small scale laboratory tests. These data were divided into two sets, i.e., about 70% for training MLP models and the rest (about 30%) considered for testing the trained network. MATLAB 7.0.4 software was used for this process. Therefore, the most appropriate proposed ANN model is shown in Fig. 2a.

Table 1 Physical quantities for the uplift resistance used in both ANN model and laboratory work

Material parameters	Symbol	values	Units
Soil			
Dry unit weight	γ	14.7, 18.0	kN/m^3
Relative density	I_d	Dense—85% Loose—35%	%
Pile			
Shaft diameter	D_s	30-40-50	mm
Base diameter	D_b	75-100-125-125	mm
Base angle	α	30-45-60	°
Embedment ratio	L/D_b	0-1-2-3-4-5	–

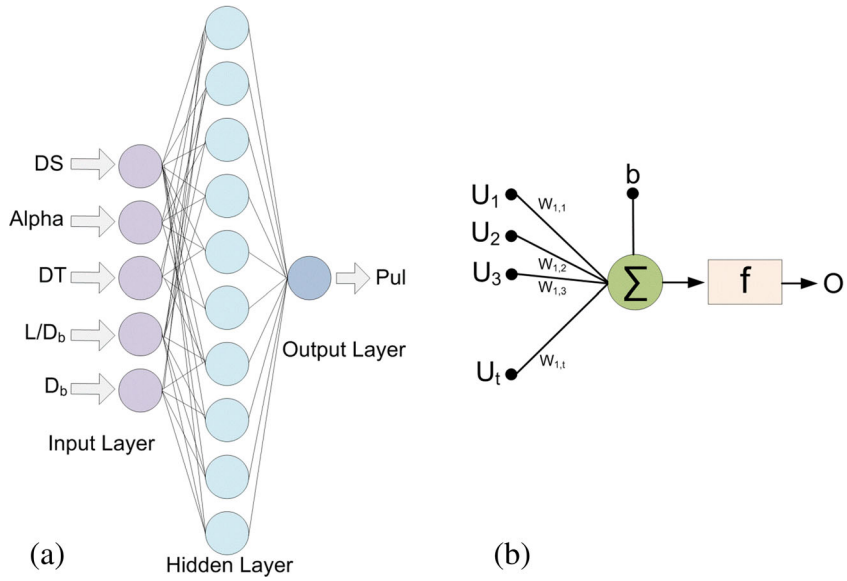

Fig. 2 **a** Proposed ANN model. **b** Mathematic model of a neuron

4 Results and discussion

As stated earlier, in training process algorithm, many different MLP structure were tested and trained by changing number of epochs, number of hidden layers, number of neurons in each hidden layer, and the training algorithm. Results from the predicted and measured data for both training and testing dataset are compared. At the end of this process, the most suitable ANN model was selected with respect to the minimum error calculated from three common error evaluation methods: (i) root mean square error (RMSE), (ii) mean absolute error (MAE), and (iii) correlation factor (CF). In addition, the connection weights and bias were thoroughly adjusted. Therefore, by using Eqs. (1) and (2), we can obtain an equation between base diameter D_b, angle of enlarged base (α), shaft diameter

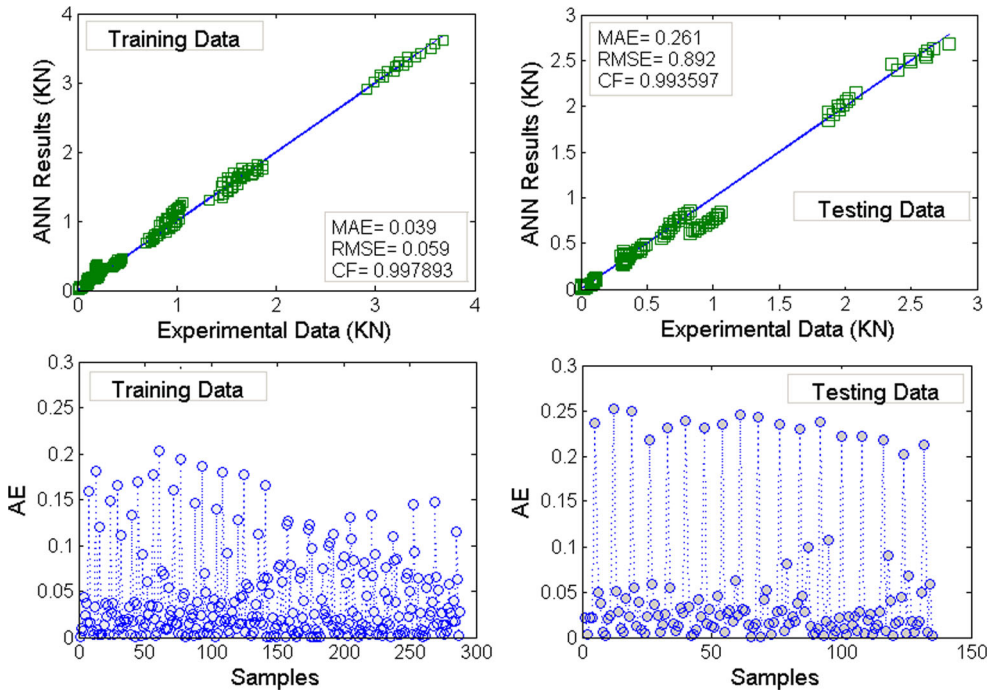

Fig. 3 Training and testing results of the proposed ANN model

Table 2 Measured and predicted (ANN) ultimate uplift resistance, P_{ul} (kN), for various D_s, D_b, and L/D_b in dense sand

D_s (mm)	Alpha ($\alpha°$)	Embedment ratio, L/D_b	D_b = 150 mm		D_b = 125 mm		D_b = 100 mm		D_b = 75 mm	
			D_b = 150-LAB	D_b = 150-ANN	D_b = 125-LAB	D_b = 125-ANN	D_b = 100-LAB	D_b = 100-ANN	D_b = 75-LAB	D_b = 75-ANN
30	45	0	0.00	0.01	0.00	0.00	0.00	0.01	0.00	0.00
30	45	1	0.13	0.15	0.10	0.09	0.05	0.06	0.02	0.01
30	45	2	0.67	0.67	0.39	0.39	0.19	0.19	0.08	0.09
30	45	3	1.72	1.71	0.99	0.99	0.50	0.53	0.21	0.22
30	45	4	3.28	3.26	2.01	2.01	1.04	1.04	0.44	0.41
30	45	5	4.34	4.32	3.08	3.06	1.87	1.84	0.78	0.79
40	45	0	0.00	0.00	0.00	0.00	0.00	0.00	0.00	0.01
40	45	1	0.13	0.14	0.10	0.09	0.04	0.06	0.02	0.01
40	45	2	0.64	0.65	0.38	0.37	0.18	0.18	0.08	0.08
40	45	3	1.66	1.68	0.98	0.96	0.55	0.55	0.20	0.22
40	45	4	3.18	3.19	1.95	1.96	1.02	1.01	0.42	0.43
40	45	5	4.43	4.45	2.98	2.99	1.82	1.79	0.75	0.76
50	45	0	0.00	0.00	0.00	0.00	0.00	0.01	0.00	0.00
50	45	1	0.12	0.13	0.10	0.09	0.04	0.06	0.02	0.02
50	45	2	0.63	0.64	0.36	0.36	0.17	0.17	0.08	0.08
50	45	3	1.62	1.62	0.94	0.94	0.55	0.55	0.19	0.21
50	45	4	3.05	3.08	1.88	1.90	0.99	0.99	0.41	0.43
50	45	5	3.89	3.91	2.91	2.92	1.77	1.74	0.74	0.73
30	30	0	0.00	0.01	0.00	0.01	0.00	0.00	0.00	0.01
30	30	1	0.13	0.15	0.11	0.09	0.05	0.06	0.02	0.02
30	30	2	0.70	0.69	0.40	0.41	0.20	0.20	0.09	0.11
30	30	3	1.81	1.79	1.03	1.03	0.50	0.50	0.22	0.23
30	30	4	3.41	3.40	2.08	2.08	1.06	1.05	0.45	0.43
30	30	5	5.42	5.37	3.68	3.68	1.87	1.89	0.82	0.85
40	30	0	0.00	0.01	0.00	0.00	0.00	0.01	0.00	0.00
40	30	1	0.13	0.14	0.12	0.09	0.05	0.06	0.02	0.02
40	30	2	0.68	0.67	0.39	0.39	0.19	0.20	0.09	0.09
40	30	3	1.76	1.77	1.00	1.00	0.50	0.50	0.22	0.22
40	30	4	3.33	3.33	2.03	2.02	1.04	1.04	0.44	0.43
40	30	5		5.35	3.60	3.61	1.82	1.85	0.81	0.81
50	30	0	0.00	0.00	0.00	0.00	0.00	0.00	0.00	0.00
50	30	1	0.13	0.13	0.11	0.09	0.04	0.07	0.02	0.02
50	30	2	0.66	0.66	0.38	0.38	0.18	0.20	0.08	0.08
50	30	3	1.72	1.71	0.98	0.97	0.50	0.50	0.21	0.21
50	30	4	3.22	3.22	1.98	1.97	1.01	1.01	0.43	0.43
50	30	5	5.31	5.29	3.56	3.55	1.79	1.80	0.79	0.78
30	60	0	0.00	0.00	0.00	0.00	0.00	0.00	0.00	0.00
30	60	1	0.13	0.12	0.10	0.09	0.04	0.06	0.02	0.01
30	60	2	0.65	0.66	0.37	0.37	0.18	0.18	0.08	0.07
30	60	3	1.68	1.67	0.96	0.96	0.50	0.50	0.21	0.20
30	60	4	3.20	3.20	1.95	1.97	1.00	1.00	0.42	0.41
30	60	5	3.97	3.96	3.45	3.44	1.76	1.77	0.74	0.74
40	60	0	0.00	0.00	0.00	0.00	0.00	0.00	0.00	0.01
40	60	1	0.12	0.12	0.09	0.09	0.04	0.06	0.02	0.01
40	60	2	0.63	0.63	0.36	0.36	0.18	0.17	0.08	0.06
40	60	3	1.64	1.65	0.93	0.94	0.50	0.50	0.20	0.19
40	60	4	3.12	3.13	1.91	1.91	0.97	0.98	0.38	0.40
40	60	5	3.93	3.95	3.32	3.34	1.69	1.71	0.71	0.71
50	60	0	0.00	0.00	0.00	0.00	0.00	0.00	0.00	0.00
50	60	1	0.12	0.11	0.09	0.09	0.04	0.06	0.02	0.01
50	60	2	0.61	0.60	0.35	0.35	0.17	0.17	0.08	0.05
50	60	3	1.59	1.59	0.90	0.92	0.50	0.50	0.19	0.17
50	60	4	3.04	3.01	1.88	1.86	0.95	0.95	0.37	0.39
50	60	5	3.91	3.89	3.24	3.23	1.65	1.66	0.68	0.67

(D_s), and embedment ratio (L/D_b) as inputs and ultimate uplift resistance (P_{ul}) as output. The following terms are shown in Eq. (3); D_S, alpha (α), DT, ER, D_b, and P_{ul} stand for the shaft diameter (mm), angle of enlarged base (degree), density condition (dense and/or loose), embedment ratio (L/D_b), base diameter (D_b), and ultimate uplift

Table 3 Measured and predicted (ANN) ultimate uplift resistance, P_{ul} (kN), for various D_s, D_b, and L/D_b in loose sand

D_s (mm)	Alpha (α°)	Embedment ratio, L/D_b	D_b = 150 mm		D_b = 125 mm		D_b = 100 mm		D_b = 75 mm	
			D_b = 150-LAB	D_b = 150-ANN	D_b = 125-LAB	D_b = 125-ANN	D_b = 100-LAB	D_b = 100-ANN	D_b = 75-LAB	D_b = 75-ANN
30	45	0	0.00	0.01	0.00	0.01	0.00	0.01	0.00	0.00
30	45	1	0.09	0.10	0.05	0.05	0.03	0.03	0.01	0.01
30	45	2	0.35	0.37	0.20	0.21	0.10	0.10	0.04	0.05
30	45	3	0.84	0.83	0.50	0.53	0.25	0.25	0.10	0.10
30	45	4	1.57	1.58	0.94	0.93	0.47	0.46	0.20	0.19
30	45	5	2.67	2.69	1.56	1.57	0.80	0.80	0.36	0.35
40	45	0	0.00	0.01	0.00	0.01	0.00	0.01	0.00	0.00
40	45	1	0.09	0.08	0.05	0.05	0.03	0.03	0.01	0.01
40	45	2	0.34	0.34	0.19	0.19	0.10	0.10	0.04	0.05
40	45	3	0.79	0.80	0.48	0.49	0.24	0.24	0.10	0.10
40	45	4	1.51	1.53	0.90	0.90	0.46	0.44	0.19	0.18
40	45	5	2.62	2.60	1.52	1.51	0.76	0.77	0.35	0.33
50	45	0	0.00	0.01	0.00	0.01	0.00	0.01	0.00	0.00
50	45	1	0.08	0.08	0.05	0.05	0.02	0.02	0.01	0.01
50	45	2	0.33	0.33	0.17	0.18	0.10	0.09	0.04	0.04
50	45	3	0.76	0.77	0.45	0.48	0.23	0.23	0.09	0.09
50	45	4	1.46	1.47	0.87	0.87	0.45	0.42	0.18	0.18
50	45	5	2.36	2.36	1.46	1.45	0.73	0.74	0.33	0.32
30	30	0	0.00	0.00	0.00	0.01	0.00	0.01	0.00	0.00
30	30	1	0.10	0.10	0.06	0.06	0.03	0.03	0.01	0.01
30	30	2	0.37	0.38	0.21	0.21	0.11	0.11	0.05	0.05
30	30	3	0.87	0.85	0.53	0.55	0.26	0.26	0.11	0.11
30	30	4	1.66	1.65	0.96	0.96	0.49	0.48	0.21	0.20
30	30	5	2.79	2.79	1.62	1.61	0.83	0.83	0.38	0.36
40	30	0	0.00	0.00	0.00	0.01	0.00	0.01	0.00	0.00
40	30	1	0.09	0.09	0.05	0.05	0.03	0.03	0.01	0.01
40	30	2	0.36	0.35	0.20	0.20	0.10	0.10	0.04	0.05
40	30	3	0.82	0.82	0.54	0.56	0.24	0.25	0.10	0.10
40	30	4	1.63	1.63	0.91	0.92	0.46	0.45	0.20	0.19
40	30	5	2.62	2.62	1.56	1.56	0.77	0.78	0.36	0.35
50	30	0	0.00	0.00	0.00	0.01	0.00	0.01	0.00	0.00
50	30	1	0.09	0.09	0.05	0.05	0.03	0.02	0.01	0.01
50	30	2	0.34	0.34	0.19	0.19	0.09	0.10	0.04	0.05
50	30	3	0.80	0.80	0.53	0.56	0.22	0.24	0.10	0.10
50	30	4	1.54	1.54	0.88	0.88	0.43	0.43	0.19	0.18
50	30	5	2.49	2.49	1.47	1.47	0.72	0.72	0.34	0.32
30	60	0	0.00	0.00	0.00	0.01	0.00	0.01	0.00	0.00
30	60	1	0.09	0.10	0.05	0.05	0.03	0.03	0.01	0.01
30	60	2	0.34	0.36	0.20	0.20	0.10	0.10	0.04	0.05
30	60	3	0.81	0.80	0.52	0.53	0.24	0.24	0.10	0.10
30	60	4	1.54	1.54	0.89	0.90	0.45	0.44	0.19	0.18
30	60	5	2.60	2.60	1.50	1.50	0.77	0.77	0.34	0.33
40	60	0	0.00	0.01	0.00	0.01	0.00	0.01	0.00	0.00
40	60	1	0.09	0.08	0.05	0.05	0.02	0.02	0.01	0.01
40	60	2	0.34	0.33	0.19	0.18	0.10	0.09	0.04	0.04
40	60	3	0.78	0.78	0.47	0.49	0.23	0.23	0.09	0.09
40	60	4	1.51	1.49	0.85	0.86	0.41	0.42	0.19	0.18
40	60	5	2.50	2.51	1.43	1.43	0.74	0.72	0.33	0.32
50	60	0	0.00	0.01	0.00	0.01	0.00	0.01	0.00	0.00
50	60	1	0.08	0.08	0.05	0.05	0.02	0.02	0.01	0.01
50	60	2	0.32	0.32	0.17	0.17	0.09	0.09	0.04	0.04
50	60	3	0.74	0.75	0.52	0.53	0.22	0.22	0.09	0.09
50	60	4	1.45	1.43	0.83	0.83	0.37	0.40	0.18	0.17
50	60	5	2.40	2.39	1.33	1.34	0.69	0.68	0.31	0.30

resistance (kN), respectively. Noteworthy, the term DT = 10 is used to represent for loose sand where DT = 20 is used to introduce dense sand. Also, "tansig" is the tansig function and "abs" is a MATLAB function that returns the absolute value. Following Eq. (3), it can be directly run in MATLAB software.

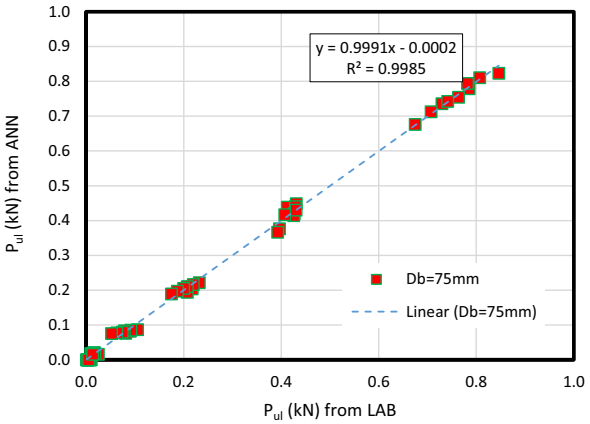

(a) D_b=75mm

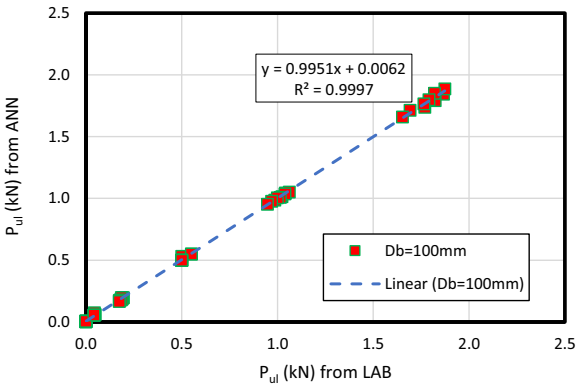

(b) D_b=100mm

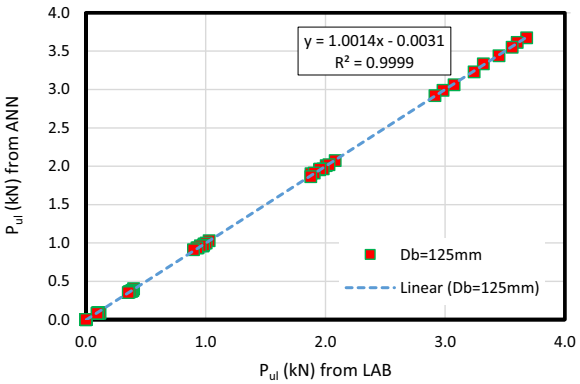

(c) D_b=125mm

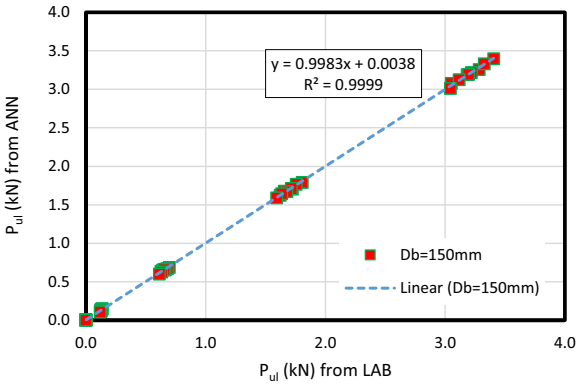

(d) D_b=150mm

◀ **Fig. 4** Comparison between measured and predicted results for various D_b in dense sand. **a** D_b = 75 mm. **b** D_b = 100 mm. **c** D_b = 125 mm. **d** D_b = 150 mm

$$\begin{aligned} D_s &= 50; \\ \text{Alpha} &= 60; \\ \text{DT} &= 20; \\ \text{ER} &= 5; \\ D_b &= 150; \end{aligned} \tag{3}$$

$$\begin{aligned} P_u\text{l} = \text{abs}(&-1.3419*\text{tansig}(0.012753*D_s - 1.4692*\text{Alpha} - \\ &0.12898*\text{DT} + 1.2804*\text{ER} + 0.65553*D\text{b} + \\ &10.8701) - 0.010131*\text{tansig}(0.27276*D_s - 0.0022046*\text{Alpha} + \\ &0.4184*\text{DT} + 1.1763*\text{ER} - 0.16275*D_b - 5.9077) + \\ &0.00083048*\text{tansig}(1.7705*D_s - 1.194*\text{Alpha} + \\ &2.0979*\text{DT} - 0.17825*\text{ER} - 0.57311*D_b + \\ &2.3419) - 1.9967*\text{tansig}(-0.00096448*D_s + \\ &0.00073819*\text{Alpha} - 0.45228*\text{DT} - 0.47458*\text{ER} + \\ &0.037422*D_b - 0.13683) + 2.7963*\text{tansig} \\ &(-0.0030848*D_s - 0.0017212*\text{Alpha} - 0.071306*\text{DT} + \\ &0.34076*\text{ER} + 0.011644*D_b - 2.1228) - 1.3461* \\ &\text{tansig}(0.002462*D_s + 1.5202*\text{Alpha} - 0.26247*\text{DT} + \\ &3.2369*\text{ER} - 0.98471*D_b + 15.6301) - 1.8572* \\ &\text{tansig}(0.00080372*D_s + 0.0018985*\text{Alpha} - \\ &0.20589*\text{DT} - 0.67674*\text{ER} + 0.035409*D_b + \\ &1.6114) - 1.8427*\text{tansig}(-0.0033276*D_s - 0.0016549* \\ &\text{Alpha} + 0.49151*\text{DT} + 0.54666*\text{ER} + 0.025507* \\ &D_b - 10.5262) - 1.8289*\text{tansig}(-0.00047678*D_s - 0.0018453*\text{A-} \\ &\text{lpha} - 0.20311*\text{DT} + 0.62268*\text{ER} - 0.038398*D\text{b} + \\ &6.8981) - 0.46146*\text{tansig}(0.0041671*D_s + 0.0040608 \\ &*\text{Alpha} + 0.18664*\text{DT} - 2.7405*\text{ER} - 0.11086*D_b + \\ &3.3236) + 2.0822) \end{aligned}$$

4.1 Discussion on ANN data

Figure 3 shows the training and testing results of proposed ANN model in comparison with the experimental data. In Fig. 3, the blue line is a reference line to show the equal relation between the measured and predicted (ANN) results and the square markers reveal exact relation between them. The absolute error (AE) is given by the following equation:

$$\text{AE} = |X_i(\text{Exp}) - X_i(\text{Pred})| \tag{4}$$

where "X(Exp)" and "X(Pred)" stand for the experimental and predicted values, respectively. Also, RMSE, MAE, and CF are given by:

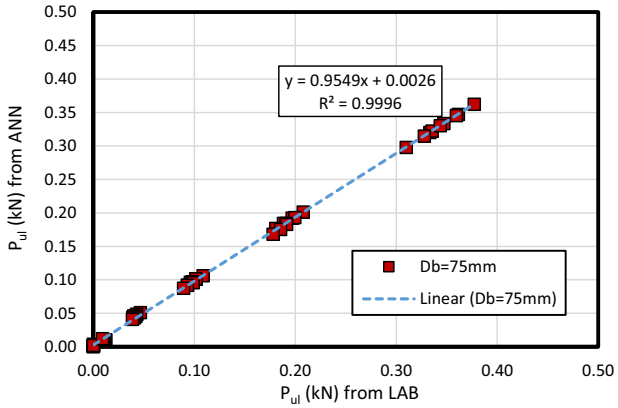

(a) D_b=75mm

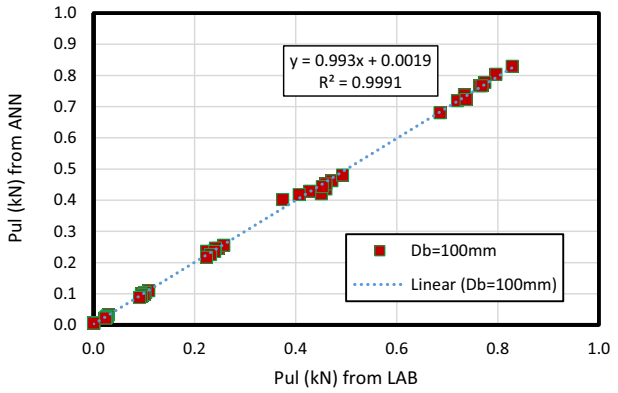

(b) D_b=100mm

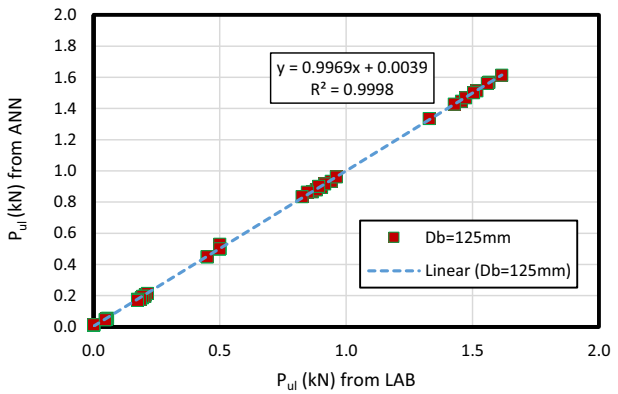

(c) D_b=125mm

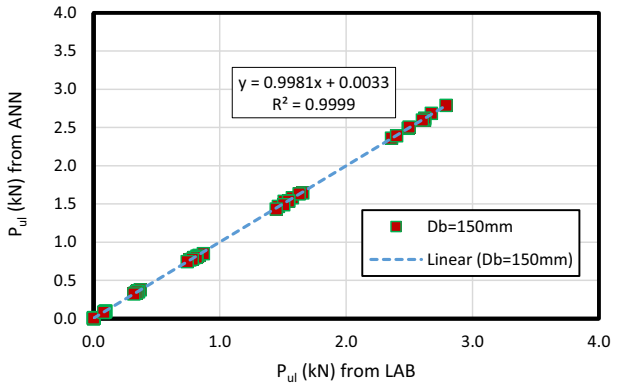

(d) D_b=150mm

◀ **Fig. 5** Comparison between measured and predicted results for various D_b in loose sand. **a** D_b = 75 mm. **b** D_b = 100 mm. **c** D_b = 125 mm. **d** D_b = 150 mm

$$\mathrm{RMSE} = \left[\frac{\sum_{i=1}^{N}\left(X_i(\mathrm{Exp}) - X_i(\mathrm{Pred})\right)^2}{N}\right]^{0.5} \tag{5}$$

$$\mathrm{MAE} = \frac{1}{N}\sum_{i=1}^{Z}\left|X_i(\mathrm{Exp}) - X_i(\mathrm{Pr\ ed})\right| \tag{6}$$

$$\mathrm{CF} = 1 - \left[\frac{\sum_{i=1}^{N}\left(X_i(\mathrm{Exp}) - X_i(\mathrm{Pred})\right)^2}{\sum_{i=1}^{N}\left(X_i(\mathrm{Exp})\right)^2}\right] \tag{7}$$

where N is the number of data. For the proposed ANN model, the obtained minimum and maximum AE for training data are 0.00003 and 0.2037, respectively. Also, for the testing data, the obtained minimum and maximum AE are 0.00059 and 0.262, respectively. From these results, it is clear that the proposed ANN model results are close to the experimental with a minimum error.

4.2 Discussion on measured data

In this section, results of uplift load capacity for a single under-reamed pile embedded in dense and loose sand are presented. The measured uplift resistance (P_{ul}) from the laboratory tests (also called LAB) along with the predicted values from the ANN approach are tabulated in Tables 2 and 3, respectively. The dataset is provided for various shaft diameter (D_s), enlarged base diameter (D_b), and L/D_b in dense and loose sand are. From these two tables, it can be found that the ultimate upload capacity of the pile (P_{ul}) increases as the L/D_b and D_b increases. These two terms are dominant factor on the uplift capacity of the under-reamed pile. Moreover, results reveal that the embedment ratio of the under-reamed pile is almost the most significant parameters. For instance, for the ANN model with D_b = 150 mm and D_s = 30 mm, the uplift load capacity of L/D_b = 1, 2, 3, 4, and 5, in dense and loose sand were 0.15, 0.67, 1.71, 3.26, and 4.32, and 0.10, 0.37, 0.83, 1.58, and 2.69 kN, respectively. The under-reamed piles are very effective way to improve the pullout forces. The presented data in Tables 2 and 3 is a good evidence to prove that the new ANN approach method shows very good agreement with measured data.

4.3 Comparison of ANN model performance

This section illustrates evaluation of ANN performance of the developed model for calculation of the uplift capacity (P_{ul}).

Figures 4 and 5 present basis of comparison where results from ANN were directly compared and related to the measured data. The ultimate uplift force (P_{ul}) for measured and predicted model, based on the change in various key parameters such as shaft diameter (D_s), under-reamed base diameter (D_b), and angle ($\alpha = 30°$, $\alpha = 45°$, and $\alpha = 60°$) along with different L/D_b ratio, are shown and compared for both of the dense and loose sand. Hence, it is first a comparison between LAB and ANN outputs for D_b equal to 75, 100, 125, and 150 mm in dense and loose sand, respectively. A simple regression on the predicted and measured results for both loose and dense sand presents R-square of almost 1.0. This reveals the accuracy of the provided ANN model. The presented model is reliable and simple where excellent agreement with the measured output in which proved that this method can be used as reliable and flexible tools to predict the ultimate uplift capacity (P_{ul}) of under-reamed base piles.

5 Conclusions

In this paper, the effects of shaft diameter, base diameter, angle of enlarged base, and embedment ratio on performance of the under-reamed single concrete piles were investigated using computational intelligence. For this purpose, a particular ANN (MLP) structure was developed. The main objective was to estimate the ultimate uplift capacity through the above input parameters with an optimized ANN model. Based on the obtained results, proposed ANN model was able to accurately predict the output with least error. The maximum AE for the training and testing data were obtained 0.2037 and 3.5000, respectively. The findings from this study prove that generated ANN model can be used as flexible and reliable solution due to their fast speed and high accuracy; therefore, it can be applied to predict the experiments precisely.

Compliance with ethical standards

Conflict of interest The authors declare that they have no conflict of interest.

References

1. Nazir R, Moayedi H, Mosallanezhad M, Tourtiz A (2015) Appraisal of reliable skin friction variation in a bored pile. Proceedings of the Institution of Civil Engineers-Geotechnical Engineering 168(1):75–86
2. Mosquera ZSZ, Tsuha CDC, Schiavon JA, Thorel L (2015) Discussion of "field investigation of the axial resistance of helical piles in dense sand". Can Geotech J 52(8):1190–1194
3. Milad F, Kamal T, Nader H, Erman O (2015) New method for predicting the ultimate bearing capacity of driven piles by using flap number. KSCE J Civ Eng 19(3):611–620
4. Arulmoli K, Martin GR, Gasparro MG, Shahrestani S, Buzzoni G (2004) Design of pile foundations for liquefaction-induced lateral spread displacements. Amer Soc Civil Engineers, New York
5. Borel S, Xv I (2001) The design of piled-raft foundations under lateral load. A a Balkema Publishers, Leiden
6. Tomlinson M, Woodward J (2008) Pile design and construction practice "5th edition". Taylor and Francis Group, New York
7. Harris DE, Madabhushi GSP (2015) Uplift capacity of an under-reamed pile foundation. Proceedings of the Institution of Civil Engineers-Geotechnical Engineering 168(6):526–538
8. Zhao N, Geng HX, Ma K, Li KN (2011) Elastic-plastic analysis on damaged multi-tower isolation structure with an enlarged base. In: Zhao JY (ed) Advances in civil engineering, pts 1–6. Trans Tech Publications Ltd, Stafa-Zurich, pp 2550–2554
9. Sego DC, Biggar KW, Wong G (2003) Enlarged base (belled) piles for use in ice or ice-rich permafrost. J Cold Reg Eng 17(2):68–88
10. Grigoryan AA, Chinenkov YA (1990) Bearing capacity and settlements of bored piles with enlarged bases in collapsible soils. Akademiai Kiado, Budapest
11. Bartholomew RF (1977) Enlarged base piles form an important class. Structural Engineer 55(12):A7–A7
12. Nazir R, Moayedi H, Pratikso A, Mosallanezhad M (2015) The uplift load capacity of an enlarged base pier embedded in dry sand. Arab J Geosci 8(9):7285–7296
13. Nazir R, Chuan HS, Niroumand H, Kassim KA (2014) Performance of single vertical helical anchor embedded in dry sand. Measurement 49:42–51
14. Sakr M (2015) Relationship between installation torque and axial capacities of helical piles in cohesionless soils. J Perform Constr Facil 29(6):11
15. Tsuha CDC, Aoki N (2010) Relationship between installation torque and uplift capacity of deep helical piles in sand. Can Geotech J 47(6):635–647
16. Briançon L, Simon B (2011) Performance of pile-supported embankment over soft soil: full-scale experiment. J Geotech Geoenviron 138(4):551–561
17. Honda T, Hirai Y, Sato E (2011) Uplift capacity of belled and multi-belled piles in dense sand. Soils Found 51(3):483–496
18. Chae D, Cho W, Na HY (2012) Uplift capacity of belled pile in weathered sandstones. International Journal of Offshore and Polar Engineering 22(4):297–305
19. Yao WJ, Chen SP (2014) Elastic-plastic analytical solutions of deformation of uplift belled pile. Teh Vjesn 21(6):1201–1211
20. Lin JG, Hsu SY, Lin SS (2015) The new method to evaluate the uplift capacity of belled piles in sandy soil. J Mar Sci Technol-Taiwan 23(4):523–533
21. Ahmadi H, Hajialilue-Bonab M (2012) Experimental and analytical investigations on bearing capacity of strip footing in reinforced sand backfills and flexible retaining wall. Acta Geotech 7(4):357–373
22. Horpibulsuk S, Niramitkornburee A (2010) Pullout resistance of bearing reinforcement embedded in sand. Soils Found 50(2):215–226
23. El Sawwaf M, Nazir A (2006) The effect of soil reinforcement on pullout resistance of an existing vertical anchor plate in sand. Comput Geotech 33(3):167–176
24. Tafreshi SNM, Javadi S, Dawson AR (2014) Influence of geocell reinforcement on uplift response of belled piles. Acta Geotech 9(3):513–528
25. Suman S, Das SK, Mohanty R (2016) Prediction of friction capacity of driven piles in clay using artificial intelligence techniques. Int J Geotech Eng 10(5):469–475
26. Momeni E, Nazir R, Armaghani DJ, Maizir H (2015) Application of artificial neural network for predicting shaft and tip resistances of concrete piles. Earth Sci Res J 19(1):85–93

27. Shahin MA (2016) State-of-the-art review of some artificial intelligence applications in pile foundations. Geosci Front 7(1):33–44
28. Shahin MA (2014) Artificial intelligence for modeling load-settlement response of axially loaded bored piles. Crc Press-Taylor & Francis Group, Boca Raton
29. Kordjazi A, Nejad FP, Jaksa MB (2014) Prediction of ultimate axial load-carrying capacity of piles using a support vector machine based on CPT data. Comput Geotech 55:91–102
30. Baziar MH, Kashkooli A, Saeedi-Azizkandi A (2012) Prediction of pile shaft resistance using cone penetration tests (CPTs). Comput Geotech 45:74–82
31. Alkroosh I, Nikraz H (2014) Predicting pile dynamic capacity via application of an evolutionary algorithm. Soils Found 54(2):233–242
32. Zhang CH, Yang SQ, Zhang JG, Xie JH, Zhang JL (2010) The numerical simulation of low strain dynamic response for foundation piles and the application for defect diagnosis by artificial neural networks. Science Press Beijing, Beijing
33. Tarawneh B, Imam R (2014) Regression versus artificial neural networks: predicting pile setup from empirical data. KSCE J Civ Eng 18(4):1018–1027
34. Hanna AM, Morcous G, Helmy M (2004) Efficiency of pile groups installed in cohesionless soil using artificial neural networks. Can Geotech J 41(6):1241–1249
35. Nejad FP, Jaksa MB, Kakhi M, McCabe BA (2009) Prediction of pile settlement using artificial neural networks based on standard penetration test data. Comput Geotech 36(7):1125–1133
36. Liang BL, Gao Y, Zhu L, Lv GB, Li X (2005) Prediction of pile displacement using PSO algorithm and artificial neural networks. China Univ Geosciences Press, Wuhan
37. Rahman M, Wang J, Deng W, Carter J (2001) A neural network model for the uplift capacity of suction caissons. Comput Geotech 28(4):269–287
38. Ardalan H, Eslami A, Nariman-Zadeh N (2009) Piles shaft capacity from CPT and CPTu data by polynomial neural networks and genetic algorithms. Comput Geotech 36(4):616–625
39. Alavi AH, Aminian P, Gandomi AH, Esmaeili MA (2011) Genetic-based modeling of uplift capacity of suction caissons. Expert Syst Appl 38(10):12608–12618
40. Cheng M-Y, Cao M-T, Tran D-H (2014) A hybrid fuzzy inference model based on RBFNN and artificial bee colony for predicting the uplift capacity of suction caissons. Autom Constr 41:60–69
41. Hagan M, Demuth H, Beale M (1996) Neural network design. PWS Pub, Boston **ISBN 7-111-10841-8**
42. Fierro R, Lewis F (1999) Multilayer feedforward networks are universal approximators. IEEE Trans Syst Man, Cybern 29(6):649–654